JOURNAL OF PETROLOGY | VOLUME 46 | NUMBER 9 | PAGES 1881–1892 | 2005 | doi:10.1093/petrology/egi038

An Experimental Study of Fe–Al Solubility in the System Corundum–Hematite up to 40 kbar and 1300°C

A. FEENSTRA[1]*, S. SÄMANN[2] AND B. WUNDER[1]

[1]GEOFORSCHUNGSZENTRUM POTSDAM, DEPARTMENT 4, TELEGRAFENBERG, D-14473 POTSDAM, GERMANY

[2]FREIE UNIVERSITÄT BERLIN, DEPARTMENT OF EARTH SCIENCES, MALTESERSTRASSE 74–100, D-12249 BERLIN, GERMANY

RECEIVED AUGUST 9, 2004; ACCEPTED MARCH 16, 2005
ADVANCE ACCESS PUBLICATION JUNE 13, 2005

The mutual solubility in the system corundum–hematite [α-$(Al, Fe^{3+})_2O_3$] was investigated experimentally using both synthetic and natural materials. Mixtures of γ-Al_2O_3 and α-Fe_2O_3 (weight ratios of 8:2 and 10:1) were used as starting materials for synthesis experiments in air at 800–1300°C with run times of 7–34 days. Experiments at 8–40 kbar and 490–1100° C were performed in a piston-cylinder apparatus (run times of 0·8–7·4 days) using a natural diasporite consisting of 60–70 vol. % diaspore and 20–30 vol. % Ti-hematite. During the diasporite–corundite transformation, the $FeTiO_3$ component (12–18 mol %) of Ti-hematite only slightly increased, implying that oxygen fugacity was maintained at high values. Run products were studied by electron microprobe and X-ray diffraction (Rietveld) techniques. An essentially linear volume of mixing exists in the solid solution with a slight positive deviation at the hematite side. Up to 1000°C, corundum contains <4 mol % Fe_2O_3 and hematite <10 mol % Al_2O_3; at 1200° C these amounts increase to 9·3 and 17·0 mol %, respectively. At 1300°C hematite was no longer stable and α-$(Al_{0.88}Fe^{3+}_{0.12}O_3)$ coexists with the orthorhombic phase $Fe^{3+}_{0.53}Al_{0.47}O_3$. The present results agree with corundum (solvus) compositions obtained in previous studies but indicate a larger solubility of Al in hematite. The miscibility gap in the solution can be modelled with an asymmetric Margules equation with interaction parameters (2σ uncertainties): $W^H_{Cor} = 89 \pm 10$ *kJ/mol;* $W^S_{Cor} = 23 \pm 8$ *J/(Kmol);* $W^H_{Hem} = 91 \pm 14$ *kJ/mol;* $W^S_{Hem} = 14 \pm 10$ *J/(Kmol). Application of the corundum–hematite solution as a solvus geothermometer is limited because of the scarcity of suitable rock compositions.*

KEY WORDS: *corundum; hematite; corundum–hematite miscibility gap; experimental study; Margules model; metabauxite*

INTRODUCTION

Corundum (α-Al_2O_3) is the dominant mineral in bauxites and Al-rich laterites metamorphosed at medium to high metamorphic conditions (Feenstra, 1985; Yalçin, 1987). It occurs, typically in moderate amounts, in other high-grade metamorphic rocks such as pelitic granulites, Al-rich marbles, and high-pressure mafic and ultramafic rocks (e.g. Enami & Zang, 1988; Morishita *et al.*, 2001, 2004; López Sánchez-Vizcaíno & Soto, 2002; Ouzegane *et al.*, 2003; Zhang *et al.*, 2004; and references therein). Hematite (α-Fe_2O_3) is isostructural with corundum (space group *R*-3*c*); it is common in soils and oxidized metamorphic rocks, where it rarely persists up to high metamorphic grades. During metamorphism of Al-rich laterites and bauxites the oxidized nature of the protoliths is commonly preserved. This may result in the coexistence of the rhombohedral oxides corundum and Al–(Ti)-hematite, thus allowing the study of their mutual solubility relations in natural systems.

Both hematite and corundum are important compounds for the production of industrial materials and ceramics. Several recent studies have focused on the synthesis, including micron- to nanosized particles, of Al-substituted hematite and Fe-substituted corundum using a variety of precursors and methods (e.g. Bouree *et al.*, 1996; Polli *et al.*, 1996; Van San *et al.*, 2001; Wells *et al.*, 2001; Da Costa *et al.*, 2002; Majzlan *et al.*, 2002; Cornell & Schwertmann, 2003). Although 'dry' experiments in the Al–Fe–O system typically suffer from sluggish reaction at temperatures below 1000°C, the system was already investigated in the early days of experimental petrology at 1 bar and up to temperatures of 1725°C

*Corresponding author. Telephone: 0 (331) 288-1415. Fax: 0 (331) 288-1402. E-mail: feenstra@gfz-potsdam.de

(Muan & Gee, 1956; Atlas & Sumida, 1958; Muan, 1958; Turnock & Eugster, 1962). In general, these studies revealed that there is only restricted mutual solubility between corundum and hematite with a wide miscibility gap. The corundum–hematite solvus does not close (in air and 1 bar) because of reduction of Al-hematite to Fe–Al spinel at ~1390°C and the formation of intermediate orthorhombic $FeAlO_3$ at ~1300°C (Muan & Gee, 1956). This restricts experimental investigation of the mutual corundum–hematite solubilities to these temperatures. Recently, Majzlan *et al.* (2002) determined the mixing enthalpies of various Al-hematite and Fe-corundum compositions by high-temperature calorimetry.

The present study re-investigates the Al_2O_3–Fe_2O_3 system at geologically relevant temperatures (up to 1300°C). In particular, we report data for the solubility of Fe in corundum, obtained by using synthetic oxide mixtures as well as natural Ti-hematite-containing diasporite as starting materials. Contrary to the previous studies, we included hydrous high-pressure experiments (up to 40 kbar) in piston-cylinder equipment. In the final part of this paper we will compare the derived corundum–hematite miscibility gap with data reported for natural rocks.

EXPERIMENTAL AND ANALYTICAL METHODS

Experimental

Mixtures of γ-Al_2O_3 and α-Fe_2O_3 were prepared with Al_2O_3:Fe_2O_3 weight ratios of 8:2 and 10:1. We used γ-Al_2O_3 because this is more reactive than α-Al_2O_3. The oxide mixtures were pressed to 5–8 mm long circular tablets ($\varnothing = 5$ mm) and heated in a three-zone horizontal furnace that was open to air. Experiments were carried out at temperatures ranging from 800 to 1300°C and lasted between 7 and 34 days (Table 1). Experimental temperature was monitored by two Pt–$PtRh_{87}$ thermocouples, between which the samples were located. Especially at the lower temperatures, run products were reground several times to promote reactivity. Runs were terminated by pulling the holder with samples and thermocouple into the cold part of the tube furnace; this resulted in cooling of the samples to <200°C within 30–40 s.

Experiments at pressures of 8–40 kbar and temperatures of 490–1100°C were performed in a piston-cylinder apparatus using a natural diasporite from Samos (Greece) as starting material. The diasporite consists of 60–70 vol. % diaspore, 20–30 vol. % Ti-hematite (12–18 mol % $FeTiO_3$ in solid solution) and minor amounts of rutile, white K-Na mica and chloritoid. The chemical composition of the diasporite, determined by standard X-ray fluorescence (XRF) methods, is as follows (in wt %): SiO_2 8·4; Al_2O_3 58·2; TiO_2 2·94; Fe_2O_3 21·2 (total Fe as Fe_2O_3); MnO 0·10; MgO 0·34; K_2O 0·85; Na_2O 0·24; CaO 0·23; P_2O_5 0·07; H_2O 8·2. The diasporite sample was encapsuled in a cold-sealed Au capsule ($\varnothing = 5$ mm, length = 10 mm). The high-pressure assembly consisted of the capsule, rock salt, a steel-furnace, and a mantled chromel–alumel thermocouple for monitoring the temperature. Further experimental details of the piston-cylinder experiments have been given by Feenstra & Wunder (2002).

Electron microprobe analysis

Chemical compositions of corundum and hematite in all 30 experiments were determined by wavelength-dispersive electron microprobe analysis (EMPA) using a CAMECA SX-100 electron microprobe. The machine was operated at 15 kV with a beam current of 20 nA and spot size of 1–2 μm. Counting times were 30–60 s on peaks; backgrounds were counted for 15–30 s. The following synthetic minerals were used as standards: corundum (Al Kα); hematite (Fe Kα); eskolaite (Cr Kα); wollastonite (Si Kα, Ca Kα); rutile (Ti Kα), periclase (Mg Kα); pyrophanite (Mn Kα, Ti Kα). The spectrometer intensity data were corrected with the PAP program (Pouchou & Pichoir, 1985).

X-ray diffraction

Run products of all 1 bar experiments and six piston-cylinder experiments were investigated by X-ray powder diffraction (Table 1). The patterns were collected using a STOE STAPI P diffractometer in the 2Θ range 5–125° for Cu$K_{\alpha 1}$ radiation. For quantitative phase analyses and for determination of the cell dimensions, Rietveld analyses were performed using the GSAS software package (Larson & Von Dreele, 1987). Initial structure models for corundum, hematite and $FeAlO_3$ used the structural parameters of Oetzel & Heger (1999), Blake *et al.* (1966) and Bouree *et al.* (1996), respectively. The lattice parameters of synthesized corundum and hematite were easily refined with the Rietveld method; χ^2 ranged from 1·0 to 1·5 and the Durbin–Watson factor from 1·8 to 1·1. Although this indicates that the calculated standard deviations are reliable, uncertainties for lattice parameters listed in Table 1 are standard deviations multiplied by three.

RESULTS AND DISCUSSION

'Dry' vs hydrous synthesis of $(Al,Fe)_2O_3$ phases

As mentioned above, two types of synthesis experiments have been performed. The first type involved the synthesis of $(Al,Fe)_2O_3$ phases from oxide mixtures in 1 bar

Table 1: Experimental conditions, chemical compositions and volume data of synthesized $(Al,Fe^{3+})_2O_3$ phases

Exp. number	Starting material	*P* (kbar)	*T* (°C)	Duration (days)	Corundum		Hematite			Corundum unit cell dimensions			Hematite unit cell dimensions		
					$Fe^{3+}/(Fe^{3+}+Al)$ molar ratio	No. of analyses	$XFeTiO_3$ mole fraction	$Fe^{3+}/(Fe^{3+}+Al)$ molar ratio	No. of analyses	*a* (Å)	*c* (Å)	Volume (Å^3)	*a* (Å)	*c* (Å)	Volume (Å^3)
Cor3a	10:1*	0·001	800	28	0·004 (2)	19		0·980 (20)	19	4·7637 (5)	13·005 (2)	255·60 (5)	5·0341 (4)	13·746 (2)	301·67 (6)
Cor3b	8:2*	0·001	800	28	0·010 (5)	24		0·974 (26)	15	4·7684 (6)	13·012 (3)	256·23 (7)	5·0338 (4)	13·744 (2)	301·60 (6)
Cor5a	10:1*	0·001	900	34	0·023 (3)	13		0·944 (39)	12	4·7633 (2)	13·0021 (8)	255·48 (3)	5·0231 (5)	13·700 (2)	299·3 (1)
Cor5b	8:2*	0·001	900	34	0·025 (8)	7		0·946 (34)	7	4·7641 (2)	13·0025 (7)	255·58 (3)	5·0232 (3)	13·708 (1)	299·56 (3)
Cor1a	10:1*	0·001	1000	7	0·023 (12)	17		0·908 (24)	18	4·7659 (2)	13·0074 (7)	255·87 (2)	5·0178 (5)	13·687 (2)	298·44 (6)
Cor1b	8:2*	0·001	1000	7	0·025 (5)	18		0·933 (17)	18	4·7696 (3)	13·016 (1)	256·43 (4)	5·0170 (4)	13·686 (1)	298·33 (5)
Cor7	8:2*	0·001	1000	21	0·039 (9)	15		0·910 (11)	15	4·7683 (1)	13·011 (1)	256·19 (1)	5·0150 (2)	13·680 (1)	297·96 (1)
Cor4a	10:1*	0·001	1100	15	0·047 (10)	17		0·864 (15)	16	4·7752 (2)	13·0270 (7)	257·25 (2)	n.d.		
Cor4b	8:2*	0·001	1100	15	0·076 (11)	15		0·872 (8)	19	4·7828 (3)	13·043 (1)	258·40 (3)	5·0045 (4)	13·645 (2)	295·95 (5)
Cor2a	10:1*	0·001	1200	7	0·058 (10)	17		0·826 (14)	19	4·7768 (1)	13·0315 (4)	257·51 (1)	n.d.		
Cor2b	8:2*	0·001	1200	7	0·093 (5)	18		0·837 (5)	20	4·7857 (2)	13·0498 (7)	258·84 (2)	4·9965 (5)	13·618 (2)	294·41 (5)
Cor6a	10:1*	0·001	1300	11	0·058 (6)	17		n.p.		4·7766 (1)	13·0303 (5)	257·46 (2)	n.p.		
Cor6b	8:2*	0·001	1300	11	0·115 (6)	17		0·532 (12)†	19	4·7941 (2)	13·0698 (6)	260·14 (2)	4·99 (1)†	$b = 8·56$ (2)† $c = 9·25$ (2)†	395·2 (7)†
AFD07	diasp‡	8	490	7·4	0·009 (1)	5	0·140 (10)§	>0·998§	8	n.d.			n.d.		
AFD03	diasp‡	17	620	5·3	0·015 (3)	9	0·144 (11)	>0·997	4	n.d.			n.d.		
AFD04	diasp‡	17	620	6·2	0·018 (2)	4	0·164	>0·998	1	n.d.			n.d.		
AFD10	diasp‡	24	600	5·6	0·015 (1)	2	0·127	>0·998	2	n.d.			n.d.		
AFD09	diasp‡	24	700	6·0	0·020 (2)	7	0·153 (19)	>0·993	6	n.d.			n.d.		
AFD13	diasp‡	30	650	6·8	0·017 (2)	6	0·180 (70)	>0·989	8	4·7637 (2)	13·005 (1)	255·57 (4)	5·0440 (6)	13·797 (3)	303·99 (8)
AFD12	diasp‡	30	700	2·5	0·019 (4)	4	0·121 (6)	>0·996	7	n.d.			n.d.		
AFD11	diasp‡	30	750	2·8	0·021 (3)	6	0·126 (18)	>0·985	8	n.d.			n.d.		
AFD01	diasp‡	30	800	5·7	0·019 (2)	7	0·161 (31)	>0·984	7	n.d.			n.d.		
AFD02	diasp‡	30	800	4·8	0·022 (3)	14	0·313 (86)	0·970 (10)	12	n.d.			n.d.		
AFD18	diasp‡	30	900	1·8	0·022 (4)	9	0·204 (50)	0·951 (8)	9	n.d.			n.d.		
Cor10	diasp‡	35	1100	0·8	0·045 (6)	14	0·179 (16)	0·879 (5)	10	4·7739 (9)	13·025 (3)	257·08 (9)	5·0229 (5)	13·730 (2)	299·99 (7)
AFD15	diasp‡	40	700	4·7	0·017 (2)	4	0·153 (32)	>0·992	3	4·7644 (3)	13·004 (1)	255·64 (4)	5·0445 (5)	13·805 (3)	304·24 (8)
AFD05	diasp‡	40	750	6·4	0·019 (3)	10	0·319 (126)	0·976 (4)	14	4·7637 (2)	13·003 (1)	255·55 (3)	5·0515 (7)	13·842 (4)	305·90 (8)
AFD16	diasp‡	40	800	2·9	0·023 (1)	8	0·132 (31)	>0·992	7	n.d.			n.d.		
AFD17	diasp‡	40	900	1·1	0·027 (4)	7	0·151 (9)	0·964 (5)	8	4·766 (2)	13·010 (1)	255·9 (2)	5·034 (2)	13·783 (1)	302·5 (2)
AFD14	diasp‡	40	950	1·5	0·028 (6)	14	0·179 (30)	0·950 (10)	12	4·7660 (2)	13·007 (1)	255·87 (4)	5·0332 (4)	13·763 (2)	301·94 (5)

Values in parentheses for compositional data represent one standard deviation of the mean in terms of the last digit(s) given; those for unit cell data three standard deviation of the mean in terms of the last digit(s) given. n.d., not determined; n.p., not present.
*Weight ratio Al_2O_3/Fe_2O_3.
†Orthorhombic $AlFeO_3$.
‡Starting material is a natural diasporite from Samos containing 60–70 vol. % diaspore, 20–30 vol. % Ti-hematite ($XFeTiO_3 = 0·12–0·18$) and minor amounts of white K-Na mica, chloritoid and rutile.
§$FeTiO_3$ (ilmenite) and Al_2O_3 (corundum) components in hematite solid solution were calculated assuming ideal stoichiometry.

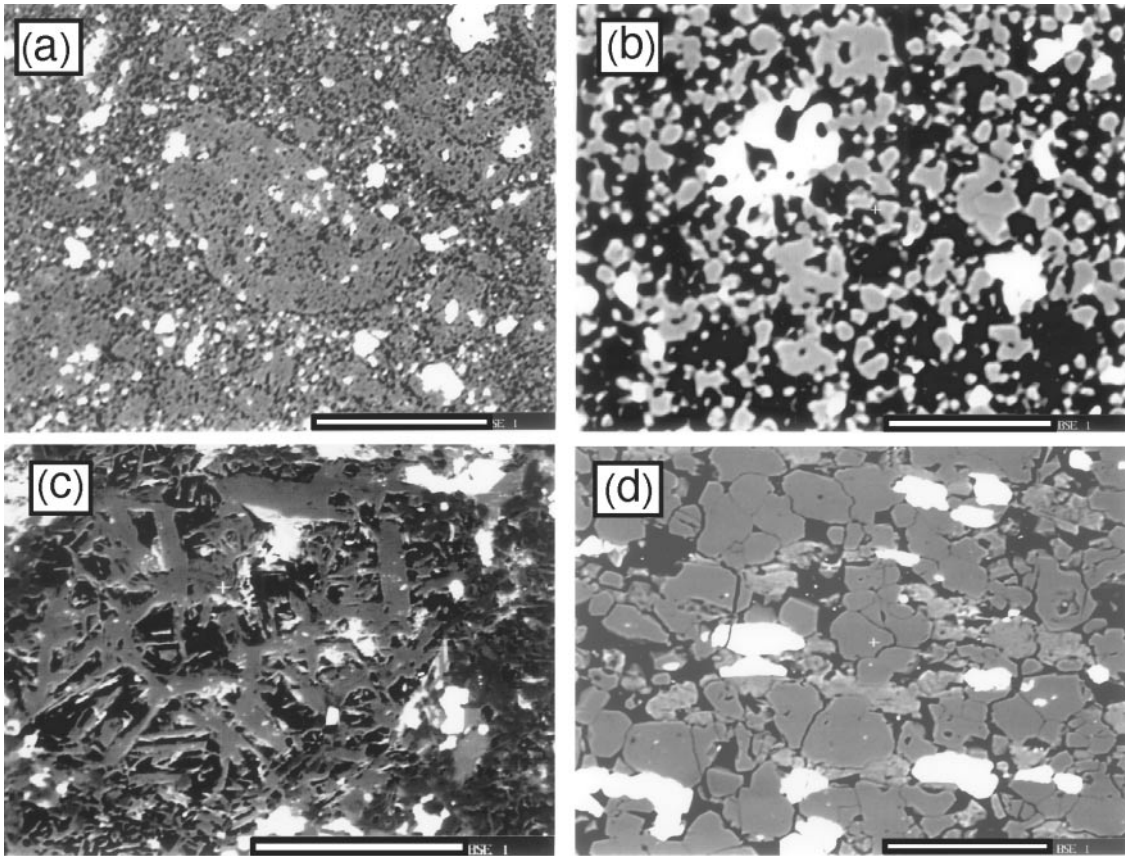

Fig. 1. Backscattered electron micrographs of run products. Pores are black in all four micrographs. (a) Fe-corundum (grey) crowded with pores coexisting with Al-hematite (bright) in run Cor7 (1 bar, 1000°C, 21 days). (b) Orthorhombic $FeAlO_3$ phase (bright) and Fe-corundum (grey) in run Cor6b (1 bar, 1300°C, 11 days). (c) Platy corundum (middle grey) and Ti-hematite (bright) in run AFD07 (8 kbar, 490°C, 7·4 days); some fine-grained diaspore (dark grey) occurs in lower right corner. (d) Fe-corundum (middle grey), Ti-hematite (bright) and muscovite (small light grey grains) in run AFD15 (40 kbar, 700°C, 4·7 days). Scale bars represent 50 μm in (a), (b) and (d), and 100 μm in (c).

furnace experiments in air. Corundum in these experiments is generally xenoblastic; pores are ubiquitous within and between the grains (Fig. 1a and b), complicating EMPA. The grain size of corundum and hematite in the 'dry' 1 bar syntheses is commonly <20 μm; at $T \geq 1000$°C local grain coarsening occurred, leading to porous corundum grains of up to 60 μm in diameter (Fig. 1a). The grain size of Al-hematite slightly increases with run temperature and reaches 30 μm at the highest temperatures. In contrast to corundum, the hematite grains are nearly devoid of pores.

The second type of experiments involved the hydrous synthesis of corundum and coexisting Ti–Al-hematite using a natural diasporite as starting material. These piston-cylinder runs have been performed in the context of a larger experimental study investigating phase relations and metasomatic interactions in a reacting diasporite–dolomite rock system (Feenstra & Wunder, 2002, and in preparation). Corundum in the hydrous syntheses forms sub-idioblastic crystals displaying a platy hexagonal habit (Fig. 1c and d). Even at the lowest synthesis temperatures (e.g. run AFD07: 8 kbar, 490°C; see Fig. 1c) the grain diameter is 10–30 μm with a crystal length of up to 50 μm. The corundum grains increase to 50–80 μm in size in the high-temperature runs. Ti–Al hematite grains are xenoblastic and 10–40 μm in diameter. Optical studies and EMPA indicate that the hematite occasionally contains lamellae of rutile, whereas lamellae or blebs of ilmenite are generally lacking. Individual hematite grains are homogeneous but slight differences in the ilmenite ($FeTiO_3$) component of hematite exist between grains in different parts of the experimental charge in some runs (e.g. in AFD02 and 05). In such cases the hematite in the external part of the charge (close to the gold capsule) has the highest $FeTiO_3$ component.

Inspection of Table 1 shows that all hydrothermally grown Fe-corundum is homogeneous in composition within the analytical uncertainty of the EMPA method, whereas 'dry' 1 bar synthesis at 800°C probably failed to produce equilibrium compositions during run times of 28 days. Comparison of runs Cor1b and Cor7, both at 1 bar and 1000°C, demonstrates that increasing the run

duration of 7 towards 21 days (with several regrindings) results in a significantly higher $Fe^{3+}/(Fe^{3+} + Al)$ for Fe-corundum (Table 1). For synthesis temperatures <1000°C, Al-hematite produced by the 'dry' method is in part inhomogeneous (see Table 1). In the hydrous experiments Al saturation in hematite appears to be lacking in most runs up to 800°C; at higher temperatures the $Fe^{3+}/(Fe^{3+} + Al)$ ratio of hematite is uniform with compositional uncertainties inherent to EMPA. Regarding the hydrous syntheses it should be noted that, contrary to corundum, which formed from diaspore, Ti-hematite was already present in the diasporite from Samos. The initial Ti-hematite contained 12–18 mol % $FeTiO_3$ component in solution whereas its Al_2O_3 content was <0·10 wt %. After the experiments the $FeTiO_3$ component of Ti-hematite ranged from 12 to 32 mol % with ≤20 mol % $FeTiO_3$ in 15 of 17 runs (Table 1). Because the Ti-hematite composition did not change considerably, a strong potential to drive recrystallization and Al saturation in Ti-hematite did not exist during the experiments. This could explain why in the hydrothermal runs Ti-hematite failed to become saturated with respect to Al at temperatures ≤800°C, whereas corundum probably did with respect to ferric iron.

Comparison of the overall results of the 'dry' and hydrothermal synthesis demonstrates that reactivity is greatly improved in the latter case. This is obvious from better chemical homogeneity (Table 1) and coarser grain size, particularly of corundum, in the hydrothermal runs. The difference in reaction kinetics may result not only from the presence of water as a catalytic reaction medium but also from the positive influence of high pressure on mineral growth.

Orthorhombic $FeAlO_3$ phase

At 1300°C and 1 bar, we synthesized orthorhombic $FeAlO_3$ with a molar $Fe^{3+}/(Al + Fe^{3+})$ ratio of 0·532 ± 0·012 coexisting with Fe-corundum with molar X_{Fe} of 0·115 ± 0·006 (run Cor6b; Table 1 and Fig. 1b). Our synthesis temperature of 1300°C is somewhat lower than the 1318°C reported by Muan & Gee (1956) and Muan (1958) as a minimum temperature for producing $FeAlO_3$ from Al_2O_3–Fe_2O_3 mixtures. Using bulk compositions with molar $Fe^{3+}/(Al + Fe^{3+})$ between 0·30 and 0·50, Polli *et al.* (1996) synthesized orthorhombic $FeAlO_3$ by pyrolysis of Al- and Fe^{3+}-nitrates at temperatures as low as 700°C. The poorly crystalline orthorhombic phase, coexisting with γ-$(Al,Fe)O_3$ solid solution, probably formed metastably. During subsequent annealing at 900–1000°C the orthorhombic phase disappeared and the run products recrystallized to stable α-$(Al,Fe)O_3$ solid solutions. Polli *et al.* (1996) succeeded in synthesizing stable orthorhombic $FeAlO_3$ at 1350°C, which is in agreement with the phase diagram of Muan & Gee (1956). Majzlan *et al.* (2002) used a similar synthesis temperature to produce $FeAlO_3$ for their calorimetric studies. On the basis of thermodynamic analysis they argued that $FeAlO_3$ is unstable at 298 K with respect to corundum and hematite, and becomes entropy-stabilized at high temperatures.

Volume–composition relations for $(Al,Fe)_2O_3$

Unit cell parameters of corundum and hematite determined by XRD are plotted versus chemical composition determined by electron microprobe in Fig. 2. Fe-corundum shows a linear relationship between composition and unit cell parameters in agreement with the findings of Majzlan *et al.* (2002). The volumes of our high-*P* Fe-corundum, grown hydrothermally at 650–950°C, tend to fall somewhat below the ideal line of mixing. Considering the compositional uncertainty (Table 1) this tendency is hardly significant. Hydrothermal Fe-corundum grown at 35 kbar and 1100°C plots again in line with 'dry' Fe-corundum synthesized from oxide mixtures at 1 bar and similar temperature.

Al-hematite shows a slight positive deviation from an ideal volume of mixing, particularly expressed by the *a* parameter (Fig. 2a). The volume–composition (*V*–*X*) relationships of our Al-hematites synthesized at 1 bar and temperatures ranging from 800 to 1200°C (Table 1) are in good agreement with the data of Majzlan *et al.* (2002) for high-*T*, Al-hematite (annealed at 1350°C and 1 bar). Volumes of low-*T*, Al-hematite prepared by Majzlan *et al.* (2002) at 702°C (and 1 bar) by thermal decomposition of Al-goethite and those of the most aluminous hematites from the studies of Van San *et al.* (2001) and Wells *et al.* (2001) display larger positive deviations from ideal mixing than our Al-hematite (Fig. 2). In the last two studies Al-hematite was synthesized from lepidocrocite (at 1 bar, 652°C) and Al-ferrihydrite gel (at 1 bar, 700°C), respectively.

Investigations of Al-substituted hematite produced at relatively low temperatures indicate that the unit cell edge *a* increases with decreasing synthesis temperature, whereas *c* remains rather constant [for a summary, see Cornell & Schwertmann (2003)]. This relationship is attributed to incorporation of structural OH^- in the hematite lattice at the lower temperatures. The hydrogen may have been inherited from the precursor phase. The loss on ignition of such hematites can be considered as a measure of initial OH^- contents. After heating to 1000°C their *a* parameters converge to a systematic relationship with $Fe^{3+}/(Al + Fe^{3+})$ as shown by our 1 bar data and the high-*T* data of Majzlan *et al.* (2002). This relationship is obtained irrespective of synthesis method (Stanjek & Schwertmann, 1992; Cornell & Schwertmann, 2003).

Our high-*P* hematite produced from natural diasporite is a ternary hematite–corundum–ilmenite solid solution containing 12–32 mol % ilmenite component (Table 1).

Because *V–X* relationships in the hematite–ilmenite solid solution are non-linear and complex (e.g. Harrison & Redfern, 2001), it seems unjustified to project the ternary volume data on the hematite–corundum binary. Therefore, we do not show lattice parameters for our high-*P* hematite in Fig. 2.

Al_2O_3–Fe_2O_3 system

Figure 3 depicts the chemical composition of corundum and hematite as a function of synthesis condition (see Table 1). We have not plotted the high-*T*, 1 bar experiments with starting Al_2O_3:Fe_2O_3 weight ratio of 10:1, in which corundum could not achieve Fe saturation and Al-hematite occurs in trace amounts (runs Cor4a and 2a; see Table 1). Likewise, Al–(Ti)-hematite compostions (runs with $T \leq 800°C$) are not shown when it is suspected that the hematite is not saturated with Al [in Table 1; $Fe^{3+}/(Fe^{3+} + Al) \geq 0{\cdot}984$]. Corundum, on the other hand, is chemically homogeneous in all hydrothermal experiments and its $Fe^{3+}/(Fe^{3+} + Al)$ increases systematically with run temperature. Hence corundum compositions are all depicted in Fig. 3.

Although oxygen fugacities were not exactly similar in the 1 bar (in air) and hydrothermal experiments, we do not observe a systematic dependence of the $Fe^{3+}/(Fe^{3+} + Al)$ of corundum on experimental approach used. Also, our results using a 'sliding' Ti-hematite + rutile internal buffer are in excellent agreement with the hydrothermal results of Turnock & Eugster (1962), who used the magnetite–hematite buffer (Fig. 3). Furthermore, Muan & Gee (1956), who studied the Al_2O_3–Fe_2O_3 system both in air and at 1 bar oxygen pressure, found only minor topological differences between the two f_{O_2} conditions. Thus it seems that oxygen fugacity in all these studies was high enough to allow 'maximum' solubility of ferric iron in corundum for the prevailing *P–T* conditions. Consequently, we treated our experimental data independently of oxygen fugacity in the thermodynamic data analysis.

Assuming that compositions of coexisting Fe-corundum and Al-hematite in the synthesis experiments

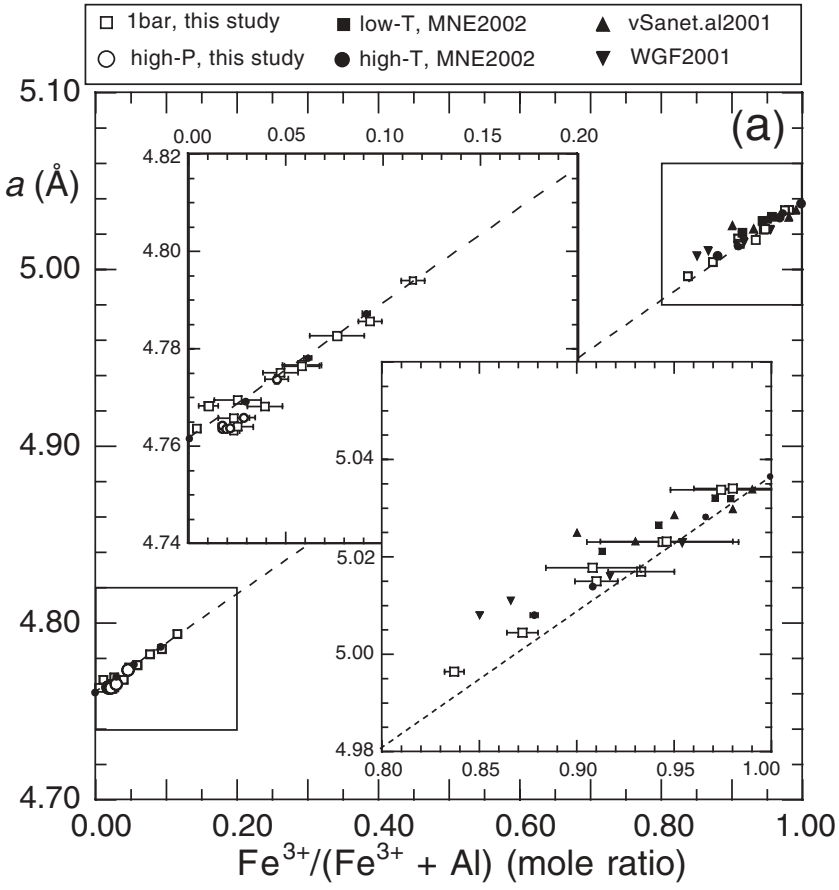

Fig. 2. Chemical composition vs unit cell parameters *a* (a), *c* (b) and unit cell volume (c) for synthetic α-$(Al,Fe)_2O_3$ phases. Insets show enlargements with error bars depicting 1σ uncertainty in chemical composition as measured by EMPA; 3σ uncertainty for unit cell parameters and volume is smaller than the plotted symbols (see Table 1). Dashed lines show linear mixing between end-members corundum and hematite. MNE2002, Majzlan *et al.* (2002); vSanet.al2001, Van San *et al.* (2001); WGF2001, Wells *et al.* (2001).

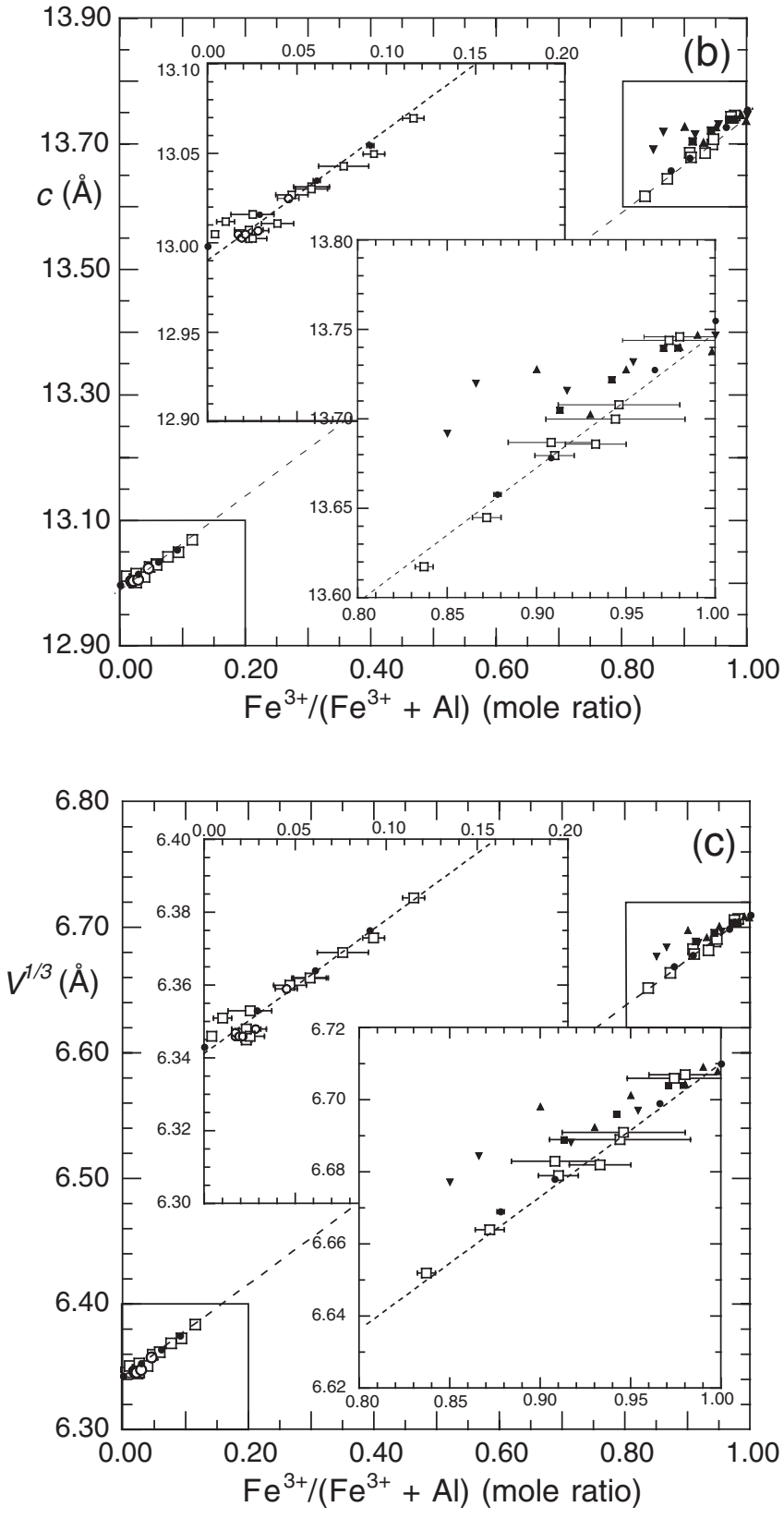

Fig. 2. Continued.

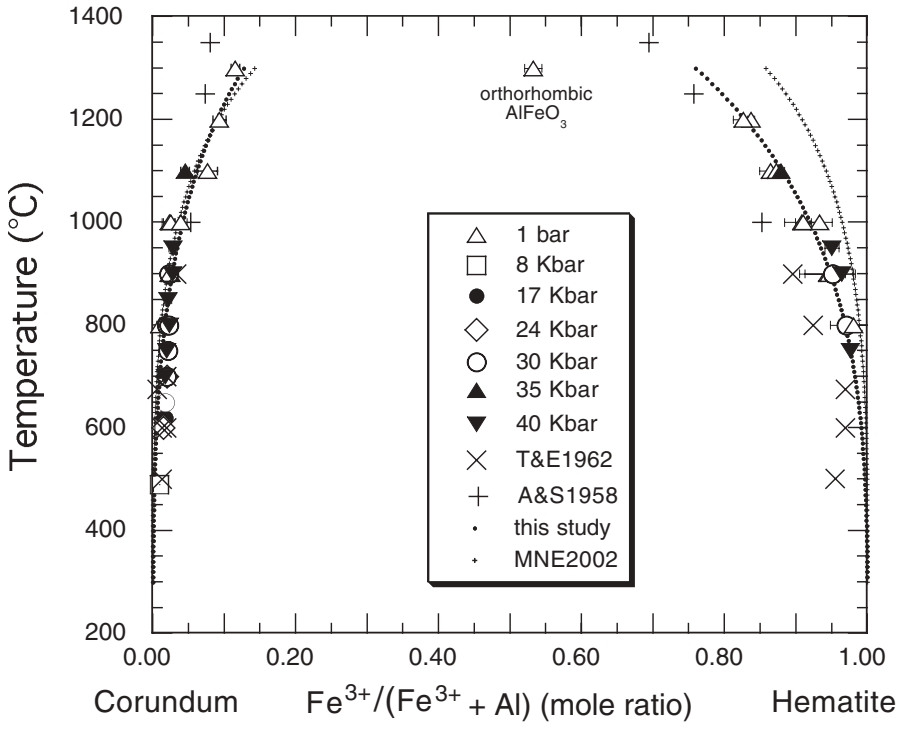

Fig. 3. Chemical compositions of Fe-corundum and Al-hematite as a function of synthesis temperature and pressure (see text). Fe-corundum in our run Cor6b (1 bar, 1300°C) coexists with orthorhombic $Fe_{1·06}Al_{0·94}O_3$ instead of Al-hematite. Results of experiments of Turnock & Eugster (1962, T&E1962) at 2 and 4 kbar and Atlas & Sumida (1958, A&S1958) at 1 bar are shown for comparison. The dotted curve shows the two-parameter Margules model fitted to our data ($W^H_{Cor} = 89 \pm 10$ kJ/mol; $W^S_{Cor} = 23 \pm 8$ J/(K mol); $W^H_{Hem} = 91 \pm 14$ kJ/mol; $W^S_{Hem} = 14 \pm 10$ J/(K mol); the curve with crosses depicts the symmetric solution model ($W^H = 116 \pm 10$ kJ/mol; $W^S = 32 \pm 4$ J/(K mol) of Majzlan *et al.* (2002, MNE2002).

represent a miscibility gap, we have fitted our data with both symmetric (one parameter) and asymmetric (two-parameter) Margules expressions, incorporating temperature dependence but ignoring pressure dependence for the interaction parameters ($W_i^G = W_i^H - TW_i^S + PW_i^v$; see, e.g. Thompson, 1967; Chatterjee, 1991; Anderson & Grerar, 1993). The PW_i^v term was neglected because the composition–volume relations for synthesized α-$(Al,Fe^{3+})_2O_3$ indicate a negligible excess volume (Fig. 2). Furthermore, the chemical compositions of coexisting Fe-corundum and Al-hematite do not vary systematically (at constant temperature) with pressure for the 0·001–40 kbar range studied. The experimental data, weighted according to their compositional uncertainty (Table 1), were fitted with the program Mathematica (Wolfram Research, Inc., 2003) using pairs of coexisting Fe-corundum and Al-hematite. An asymmetric Margules model $\{\Delta G_{mix} = X_{Hem}(1 - X_{Hem})[W^G_{Cor}X_{Hem} + W^G_{Hem}(1 - X_{Hem})]\}$, where $X_{Hem} = Fe^{3+}/(Fe^{3+} + Al)$, excellently reproduces the experimental data (Fig. 3) with the following interaction parameters (2σ uncertainties): $W^H_{Cor} = 89 \pm 10$ kJ/mol; $W^S_{Cor} = 23 \pm 8$ J/K mol; $W^H_{Hem} = 91 \pm 14$ kJ/mol; $W^S_{Hem} = 14 \pm 10$ J/K mol. Symmetric or T-independent models (only W_i^H) inadequately fitted the data.

Our results for Fe solubility in corundum concur with previous experimental studies (Muan & Gee, 1956; Atlas & Sumida, 1958; Turnock & Eugster, 1962). The first two studies of the Al_2O_3–Fe_2O_3 join were performed at 1 bar in air and temperatures ≥1000°C. In their extensive study of Fe–Al oxide phase relationships below 1000°C, Turnock & Eugster (1962) hydrothermally studied the Al_2O_3–Fe_2O_3 join at 2 and 4 kbar using the hematite–magnetite buffer. Their results for the corundum limb of the solvus are in excellent agreement with our low-T, hydrothermal experiments. For the hematite limb they determined, like Atlas & Sumida (1958), a higher Al solubility in hematite than we obtained (Fig. 3). On the other hand, Muan & Gee (1956) obtained for the range 1000–1350°C a lower Al solubility in hematite than indicated by our study. It should be kept in mind, however, that these 40–50-year-old experimental studies preceded routine electron microprobe analysis. Phase compositions were normally determined by XRD measurement using a single reflection. Using the (124) reflection of α-$(Al,Fe^{3+})_2O_3$, Turnock & Eugster (1962) indicated a compositional accuracy of ±3 wt % Al_2O_3. The accuracy of these older phase diagrams therefore should be judged in this context.

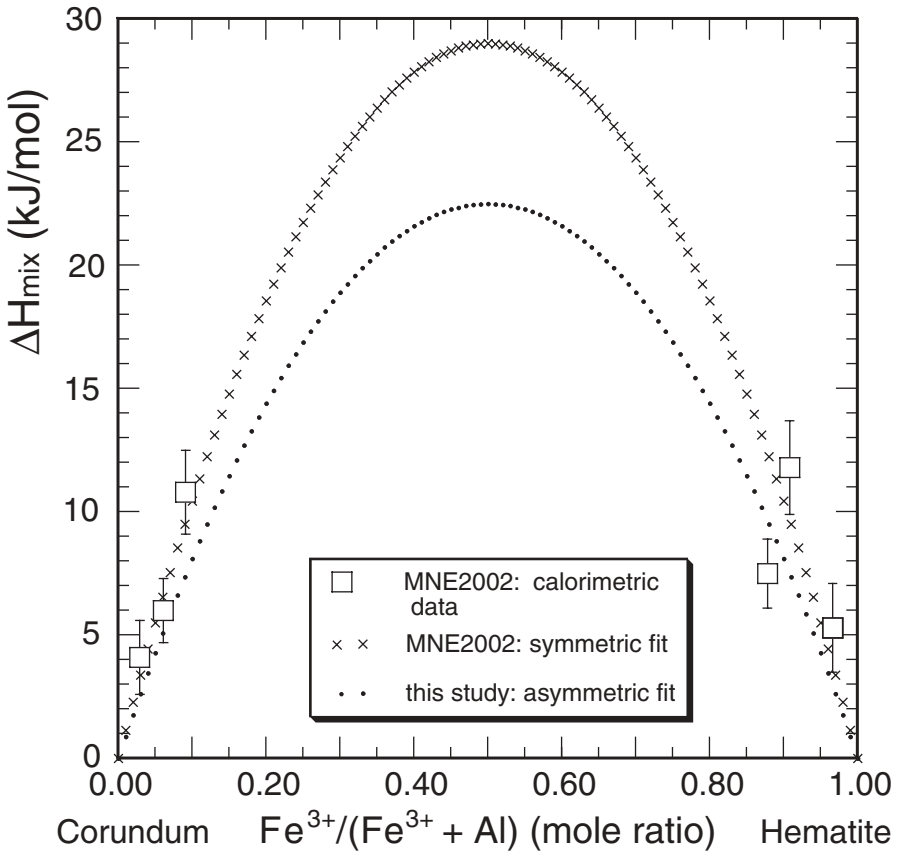

Fig. 4. ΔH_{mix} of corundum–hematite solid solution according to mixing model of present study and that of Majzlan *et al.* (2002, MNE2002). Squares (2σ error bars) indicate enthalpies of mixing measured by high-temperature oxide-melt solution calorimetry (Majzlan *et al.*, 2002).

Majzlan *et al.* (2002) determined the enthalpies of mixing of various Fe-corundum and Al-hematite solid solutions by high-temperature oxide-melt calorimetry (Fig. 4). Excluding the Al-hematites synthesized by thermal decomposition of Al-goethite at 700°C, which contained considerable amounts of H_2O, they fitted the calorimetric results with a symmetric Margules equation with $W^H = 116 \pm 10$ kJ/mol and $W^S = 32 \pm 4$ J/K mol. Compared with our results the resulting miscibility gap agrees well at the corundum limb but is clearly wider at the hematite limb of the solvus (Fig. 3). With regard to the experimental study of Muan & Gee (1956), Majzlan *et al.* (2002) noted that the deduced W parameters tend to overestimate the crest of the solvus, the exact position of which is unknown because of instability of corundum + hematite at such conditions. Fitting the phase diagram of Muan & Gee (1956) with an asymmetric T-independent Margules model, Majzlan *et al.* (2002) obtained $W^G_{Cor} = 62 \pm 4$ kJ/mol and $W^G_{Hem} = 74 \pm 4$ kJ/mol. These values approximate, for example, at 1100°C the $W^G_{Cor} = 57$ kJ/mol and $W^G_{Hem} = 72$ kJ/mol obtained in our data analysis. Our model is more asymmetric, however, and the asymmetry increases with temperature owing to the difference in W^S_{Cor} and W^S_{Hem}.

Figure 4 compares our mixing model for the corundum–hematite solid solution with that of Majzlan *et al.* (2002) and shows that within experimental uncertainties the calorimetric data also agree with our model. Majzlan *et al.* (2002) argued that the positive excess entropy required to model the miscibility gap may relate to increasing ordering for compositions approaching that of the orthorhombic $FeAlO_3$ phase. For dilute compositions close to the end-members (at low T) ordering is probably of little importance.

COMPARISON WITH NATURE

Corundum has been documented in a variety of metamorphic and magmatic rocks covering a wide field of P–T conditions ranging from the middle crust to those of the diamond stability field. Many of these occurrences are found in Fe-poor rocks commonly devoid of Fe–(Ti)-oxides with ferric iron. Such corundum typically contains $<0{\cdot}5$ wt % Fe_2O_3 and is of little significance for comparative purposes with the present study.

Owing to their Al–Fe-rich and oxidized nature, the rare occurrences of metamorphosed bauxite and Al-rich laterite are favourable to provide information on maximum Fe solubility in corundum for the prevailing metamorphic conditions. The highest Fe_2O_3 content (9·17 wt %) in natural corundum was probably reported by Agrell & Langley (1958) from such a geological environment. Those workers described yellow corundum occurring in porcellanite at a contact of a dolerite intrusion at Tievebulliagh (Northern Ireland). The corundum is associated with hematite, pseudobrookite and iron-mullite, indicating a very high oxygen fugacity during contact metamorphism of a lateritized basalt. Contact metamorphic temperatures were estimated to be between 900 and 1150°C. Assuming that the 9·17 wt % Fe_2O_3 (molar $X_{Fe} = 0{\cdot}061$) represents solvus composition, we obtain a temperature of ~1050°C when applying our corundum–hematite solution model (Fig. 3).

Another example of metabauxitic Fe-corundum containing up to 2·0–2·9 wt % (1·2–1·9 mol %) Fe_2O_3 was documented by Altenberger *et al.* (1992) and Adusumalli (1994) from the Odenwald complex (Germany). Here corundum + sillimanite + magnetite/ilmenite felses, interpreted to be metamorphosed Al-rich palaeosols, are locally present along the contact of gabbros. Using our solvus data, the Odenwald corundum yields a temperature of 650–800°C. This is lower than the 860–900°C deduced from Fe–Ti-oxide thermometry for the (~362 Ma) Seeheim contact metamorphism (Altenberger *et al.*, 1992) but falls in the range of estimated regional metamorphic conditions (Adusumalli, 1994) for the corundum occurrences in the Odenwald complex.

Corundum from the metamorphic bauxites of Naxos (Greece) contains 0·5–0·8 mol % Fe_2O_3 in solid solution at the highest P–T conditions (~6 kbar, ~700°C) reached during regional metamorphism on the island (Feenstra, 1985; A. Feenstra, unpublished results, 1983–1985). Such amounts of Fe_2O_3 are lower than implied by the present experiments for a similar temperature (Fig. 3, Table 1). The difference may indicate that at the f_{O_2} conditions of coexisting magnetite + (hemo)ilmenite in the Naxos metabauxites, there is considerably less Fe^{3+} solubility in corundum than in the more oxidized experiments. Alternatively, it is possible that the Naxos corundum is not saturated with respect to Fe^{3+} for the prevailing amphibolite-facies conditions. Corundum in the Naxos metabauxites formed during regional metamorphism by breakdown of diaspore (at ~6 kbar and ~420°C) and initially coexisted with Ti-hematite + rutile (Feenstra, 1985; Urai & Feenstra, 2001). The corundum from near the corundum-in isograd is comparable in Fe_2O_3 contents with that of the highest grade zones, and a correlation between Fe_2O_3 in corundum and metamorphic temperature on Naxos is not found (Feenstra, 1985; A. Feenstra, unpublished results, 1983–1985). It is thus possible that corundum preserved its initial $Fe^{3+}/(Fe^{3+} + Al)$ and during progressive metamorphism (rising T) failed to adapt compositionally owing to its sluggishness to equilibrate.

The minor and trace element chemistry of gem-quality corundum has been the subject of several detailed studies. Garland (2002) investigated alluvial sapphire deposits of western Montana and compared the sapphire chemistry with that of world-wide occurrences of corundum types of different metamorphic and magmatic origin. The study revealed that corundum associated with alkali basalts is highest in iron of all genetic types containing on average 7000 ppm Fe. For example, corundum from Shandong (China) and Australia (NSW regions and Queensland) contains up to 12 000–13 000 ppm Fe (~1·8 wt % Fe_2O_3). When applying our solvus data, even such Fe concentrations give unrealistically low temperatures for basaltic melts, implying that physico-chemical conditions (e.g., f_{O_2} activity of Fe^{3+}) in the magmatic systems must differ considerably from those in our experiments imposing 'maximum' Fe solubility in corundum. The iron content of gem-quality corundum from metamorphic origin widely varies but is typically lower than that of the basaltic type.

Hunstiger (1988) investigated the mineral chemistry and petrogenesis of a variety of ruby-type corundum-containing metamorphic rocks including amphibolites, Al-rich gneisses and anatexites, and metacarbonate rocks. Whereas corundum in marbles is very poor in iron, the Fe_2O_3 content of corundum in the other rock types may be up to 0·8 wt %. Such concentrations are low compared with our experimental data considering the amphibolite- to granulite-facies conditions to which the rocks have been subjected. As discussed above, the difference probably reflects much lower activity of Fe^{3+} and/or lack of chemical equilibrium in the natural rocks.

CONCLUSIONS

(1) The present experimental study confirms the results of classical (40–50 years old) investigations of the corundum–hematite system (at low P), which demonstrated that there exists a wide miscibility gap that does not close. Up to pressures of 40 kbar there is a negligible effect of pressure on the width of the solvus expressed in an insignificant excess volume for the solid solution. Our results for 'maximum' Fe solubility in corundum as a function of temperature are in excellent agreement with those of the previous studies; however, we determined a larger Al solubility in hematite.

(2) The corundum–hematite solvus has limited potential as a geothermometer bcause of the scarcity of suitable rock types for application and the restricted Fe^{3+}–Al exchange in the solution at $T \leq 1000$°C that introduces large inaccuracy in T. The sluggish nature of corundum

to re-equilibrate may also hamper application. Geothermometric application of Al solubility in hematite is even more difficult because of the extreme scarcity of hematite coexisting with corundum in metamorphic and magmatic rocks. In addition, the complex mineral chemistry of natural hematite complicates application. Nevertheless, we presented some examples of high-grade bauxitic or lateritic rocks for which realistic T estimates were obtained using our experimental calibration.

ACKNOWLEDGEMENTS

We are much obliged to Matthias Kreplin and Gerhard Berger for sample preparation, Reiner Schulz for technical help with experiments, Oona Appelt and Heike Steigert for technical assistance with characterization of run products, and Matthias Gottschalk for data fitting with Mathematica. We thank Dominique Lattard, Juraj Majzlan and an anonymous reviewer for thoughtful reviews, and Reto Gieré for his editorial handling. Their comments helped us much to improve the clarity of the manuscript.

REFERENCES

Adusumalli, C.-I. (1994). Metabauxite des Bergsträsser Odenwaldes—Petrologie, Geochemie und die geologischen Konsequenzen. Ph.D. thesis, University of Würzburg, 384 pp.

Agrell, S. O. & Langley, J. M. (1958). The dolerite plug at Tievebulliagh, near Cushendall, Co. Antrim. Part (1): The thermal metamorphism. *Proceedings of the Royal Irish Academy, Section B* **59**, 93–127.

Altenberger, U., Oberhänsli, R., Adusmalli, C. I. & Rasool, R. (1992). The corundum-bearing rocks around Seeheim in the Odenwald complex, Mid-German crystalline rise. *Zentralblatt für Geologie und Paläontologie, Teil I* **H7/8**, 895–908.

Anderson, G. M. & Grerar, D. A. (1993). *Thermodynamics in Geochemistry. The Equilibrium Model*. Oxford: Oxford University Press.

Atlas, L. M. & Sumida, W. K. (1958). Solidus, subsolidus, and subdissociation phase equilibria in the system Fe–Al–O. *Journal of the American Ceramic Society* **41**, 150–160.

Blake, R. L., Hessevick, R. E., Zoltai, T. & Finger, I. W. (1966). Refinement of the hematite structure. *American Mineralogist* **51**, 123–129.

Bouree, F., Baudour, J. L., Elbadraoui, E., Musso, J., Laurent, C. & Rousset, A. (1996). Crystal and magnetic structure of piezoelectric, ferrimagnetic and magnetoelectric aluminium iron oxide $FeAlO_3$ from neutron powder diffraction. *Acta Crystallographica (B)* **52**, 217–222.

Chatterjee, N. D. (1991). *Applied Mineralogical Thermodynamics*. Berlin: Springer, 321 pp.

Cornell, R. M. & Schwertmann, U. (2003). *The Iron Oxides: Structure, Properties, Reactions, Occurrences and Uses*, 2nd edn. Weinheim: Wiley–VCH, 664 pp.

Da Costa, G. M., Van San, E., De Grave, E., Vandenberghe, R. E., Barrón, V. & Datas, L. (2002). Al hematites prepared by homogeneous precipitation of oxinates: material characterization and determination of the Morin transition. *Physics and Chemistry of Minerals* **29**, 122–131.

Enami, M. & Zang, Q. (1988). Magnesian staurolite in garnet–corundum rocks and eclogite from the Donghai district, Jiangsu province, east China. *American Mineralogist* **73**, 48–56.

Feenstra, A. (1985). Metamorphism of bauxites on Naxos, Greece. Ph.D. thesis, University of Utrecht, 206 pp.

Feenstra, A. & Wunder, B. (2002). Dehydration of diasporite to corundite in nature and experiment. *Geology* **30**, 119–122.

Garland, M. I. (2002). The alluvial sapphire deposits of western Montana. Ph.D. thesis, University of Toronto, 400 pp.

Harrison, R. J. & Redfern, S. A. T. (2001). Short- and long-range ordering in the ilmenite–hematite solid solution. *Physics and Chemistry of Minerals* **38**, 399–412.

Hunstiger, C. (1988). Darstellung und Vergleich primärer Rubinvorkommen in metamorphen Muttergesteinen. Ph.D. thesis, University of Würzburg, 279 pp.

Larson, A. C. & Von Dreele, R. B. (1987). Generalized structure analysis system. *Los Alamos National Laboratory Report* **LA-UR-86-748**.

López Sánchez-Vizcaíno, V. & Soto, J. I. (2002). Reaction zones developed between corundum metapelite and marble, Alborán Sea basement, western Mediterranean: origin and phase relations. *Canadian Mineralogist* **40**, 85–101.

Majzlan, J., Navrotsky, A. & Evans, B. J. (2002). Thermodynamics and crystal chemistry of the hematite–corundum solid solution and the $FeAlO_3$ phase. *Physics and Chemistry of Minerals* **29**, 515–526.

Morishita, T., Arai, S. & Gervilla, F. (2001). High-pressure aluminous mafic rocks from the Ronda peridotite massif, southern Spain: significance of sapphirine- and corundum-bearing mineral assemblages. *Lithos* **57**, 143–161.

Morishita, T., Arai, S. & Green, D. H. (2004). Possible non-melted remnants of subducted lithosphere: experimental and geochemical evidence from corundum-bearing mafic rocks in the Horoman Peridotite Complex, Japan. *Journal of Petrology* **45**, 235–252.

Muan, A. (1958). On the stability of the phase $Fe_2O_3.Al_2O_3$. *American Journal of Science* **256**, 413–422.

Muan, A. & Gee, C. L. (1956). Phase equilibrium studies in the system iron oxide–Al_2O_3 in air and at 1 atm. O_2 pressure. *Journal of the American Ceramic Society* **39**, 207–214.

Oetzel, M. & Heger, G. (1999). Laboratory X-ray powder diffraction: a comparison of different geometries with special attention to the use of the CuKα doublet. *Journal of Applied Crystallography* **32**, 799–807.

Ouzegane, K., Guiraud, M. & Kienast, J. R. (2003). Prograde and retrograde evolution in high-temperature corundum granulites (FMAS and KFMASH systems) from In Ouzzal terrane (NW Hoggar, Algeria). *Journal of Petrology* **44**, 517–545.

Polli, A. D., Lange, F. E. & Levi, C. G. (1996). Crystallization behavior and microstructure evolution of $(Al, Fe)_2O_3$ synthesized from liquid precursors. *Journal of the American Ceramic Society* **79**, 1745–1755.

Pouchou, J. L. & Pichoir, F. (1985). 'PAP' φ(ρZ) procedure for improved quantitative microanalysis. *Microbeam Analysis* 104–106.

Stanjek, H. & Schwertmann, U. (1992). The influence of aluminum on iron oxides. Part XVI: Hydroxyl and aluminum substitution in synthetic hematites. *Clays and Clay Minerals* **40**, 347–354.

Thompson, J. B., Jr (1967). Thermodynamic properties of simple solutions. In: Abelson, P. H. (ed.) *Researches in Geochemistry, Vol. 2*. New York: John Wiley, pp. 340–361.

Turnock, A. C. & Eugster, H. P. (1962). Fe–Al oxides: phase relationships below 1000°C. *Journal of Petrology* **3**, 533–565.

Urai, J. L. & Feenstra, A. (2001). Weakening associated with the diaspore–corundum dehydration reaction in metabauxites: an example from Naxos (Greece). *Journal of Structural Geology* **23**, 941–950.

Van San, E., De Grave, E., Vandenberghe, R. E., Desseyn, H. O., Datas, L., Barrón, V. & Rousset, A. (2001). Study of Al-substituted hematites, prepared from thermal treatment of lepidocrocite. *Physics and Chemistry of Minerals* **28**, 488–497.

Wells, M. A., Gilkes, R. G. & Fitzpatrick, R. W. (2001). Properties and acid dissolution of metal-substituted hematites. *Clays and Clay Minerals* **49**, 60–72.

Wolfram Research, Inc. (2003). Mathematica, Version 5.0. Champaign, IL: Wolfram Research, Inc.

Yalçin, U. (1987). Petrologie und Geochemie der Metabauxite SW-Anatoliens. Ph.D. thesis, Ruhr University Bochum, 146 pp.

Zhang, R. Y., Liou, J. G. & Zheng, J. P. (2004). Ultrahigh-pressure corundum-rich garnetite in garnet peridotite, Sulu terrane, China. *Contributions to Mineralogy and Petrology* **147**, 21–31.